Baculovirus actin-rearrangement-inducing factor ARIF-1 induces the formation of dynamic invadosome clusters

Domokos I. Lauko[a], Taro Ohkawa[b], Sergio E. Mares[b,†], and Matthew D. Welch[a,b,*]
[a]Microbiology Graduate Group and [b]Department of Molecular & Cell Biology, University of California, Berkeley, Berkeley, CA 94720

ABSTRACT **The baculovirus *Autographa californica* multiple nucleopolyhedrovirus (AcMNPV), a pathogen of lepidopteran insects, has a striking dependence on the host cell actin cytoskeleton. During the delayed-early stage of infection, AcMNPV was shown to induce the accumulation of actin at the cortex of infected cells. However, the dynamics and molecular mechanism of cortical actin assembly remained unknown. Here, we show that AcMNPV induces dynamic cortical clusters of dot-like actin structures that mediate degradation of the underlying extracellular matrix and therefore function similarly to clusters of invadosomes in mammalian cells. Furthermore, we find that the AcMNPV protein actin-rearrangement-inducing factor-1 (ARIF-1), which was previously shown to be necessary and sufficient for cortical actin assembly and efficient viral infection in insect hosts, is both necessary and sufficient for invadosome formation. We mapped the sequences within the C-terminal cytoplasmic region of ARIF-1 that are required for invadosome formation and identified individual tyrosine and proline residues that are required for organizing these structures. Additionally, we found that ARIF-1 and the invadosome-associated proteins cortactin and the Arp2/3 complex localize to invadosomes and Arp2/3 complex is required for their formation. These ARIF-1–induced invadosomes may be important for the function of ARIF-1 in systemic virus spread.**

Monitoring Editor
Nihal Altan-Bonnet
National Institutes of Health, NHLBI

Received: Nov 23, 2020
Revised: May 28, 2021
Accepted: Jun 7, 2021

INTRODUCTION

Intracellular microbial pathogens are master manipulators of host cell biology and have evolved myriad strategies to hijack host cell machinery and repurpose host processes to facilitate infection. One such strategy is to hijack the host actin cytoskeleton, which can facilitate pathogen invasion, intracellular movement, and/or cell–cell spread. The baculovirus *Autographa californica* multiple nucleopolyhedrovirus (AcMNPV), an enveloped DNA virus that orally infects larval lepidopteran insects (caterpillars), is notable for manipulating the host actin cytoskeleton extensively throughout infection. Upon entry into the host cell cytoplasm, AcMNPV nucleocapsids undergo actin-based motility, using the viral P78/83 protein to activate host Arp2/3 complex to polymerize actin filaments (Goley *et al.*, 2006; Ohkawa *et al.*, 2010). Upon expression of early viral genes, actin filaments accumulate at the cortex of infected cells (Charlton and Volkman, 1991; Roncarati and Knebel-Mörsdorf, 1997; Dreschers *et al.*, 2001). This accumulation dissipates during late viral gene expression as monomeric actin is imported into and polymerizes within the nucleus (Charlton and Volkman, 1991, 1993; Volkman *et al.*, 1992; Ohkawa and Volkman, 1999; Ohkawa *et al.*, 2002; Hepp *et al.*, 2018). Newly assembled viral nucleocapsids also harness P78/83 and Arp2/3 complex to polymerize actin and are propelled to the nuclear periphery to facilitate nuclear egress (Ohkawa and Welch, 2018). As both actin polymerization in the nucleus and viral actin-based motility are required for successful viral infection (Volkman *et al.*, 1987; Volkman, 1988; Volkman and Kasman, 2000; Hess *et al.*, 1989;

This article was published online ahead of print in MBoC in Press (http://www.molbiolcell.org/cgi/doi/10.1091/mbc.E20-11-0705) on June 16, 2021.

†Present address: Center for Computational Biology, University of California, Berkeley, Berkeley, CA 94720.

*Address correspondence to: Matthew D. Welch (welch@berkeley.edu).

Abbreviations used: AcMNPV, *Autographa californica* multiple nucleopolyhedrovirus; ARIF-1, actin-rearrangement-inducing factor-1; BmNPV, *Bombyx mori* nucleopolyhedrovirus; ECM, extracellular matrix; GP64, glycoprotein 64; hpi, hours postinfection; TIRF, total internal reflection fluorescence; TKS5, tyrosine kinase with 5 SH3 domains.

© 2021 Lauko *et al.* This article is distributed by The American Society for Cell Biology under license from the author(s). Two months after publication it is available to the public under an Attribution–Noncommercial–Share Alike 3.0 Unported Creative Commons License (http://creativecommons.org/licenses/by-nc-sa/3.0).

"ASCB®," "The American Society for Cell Biology®," and "Molecular Biology of the Cell®" are registered trademarks of The American Society for Cell Biology.

Ohkawa and Volkman, 1999; Goley *et al.*, 2006), the ability of AcMNPV to hijack the host actin cytoskeleton is of critical importance.

A second AcMNPV protein that impacts the actin cytoskeleton is the actin-rearrangement-inducing factor-1 (ARIF-1) (Roncarati and Knebel-Mörsdorf, 1997). ARIF-1 is a delayed-early viral protein that was identified in a screen for AcMNPV genes that cause alterations in the actin cytoskeleton when expressed in insect cells and was shown to be necessary and sufficient to induce the accumulation of actin filaments at the plasma membrane during early infection (Roncarati and Knebel-Mörsdorf, 1997). ARIF-1 contains three predicted transmembrane domains and localizes to the plasma membrane (Dreschers *et al.*, 2001). It also contains a C-terminal domain with proline-rich sequences that is phosphorylated on tyrosine residues (Dreschers *et al.*, 2001), although the function of these sequences is unknown. The *arif-1* gene is conserved among alphabaculoviruses (Roncarati and Knebel-Mörsdorf, 1997), suggesting that it performs an important function. However, ARIF-1 is not important for viral replication in cultured cells (Dreschers *et al.*, 2001; Taka *et al.*, 2013; Kokusho *et al.*, 2015). Nevertheless, insects infected with a mutant *Bombyx mori* NPV (BmNPV; closely related to AcMNPV) lacking *arif-1* experienced delays in infection of major organ systems and death, indicating that ARIF-1 accelerates systemic infection (Kokusho *et al.*, 2015). However, the mechanisms by which ARIF-1 functions in rearrangement of the host actin cytoskeleton in cells and systemic infection in caterpillars are still unknown.

During infection in caterpillars, AcMNPV must bypass barriers to systemic infection. AcMNPV infects through the oral route and establishes initial infection in midgut epithelial cells (Rohrmann, 2019). After replication, the virus spreads from the midgut to the tracheal system (Engelhard *et al.*, 1994) and then to most major organ systems. However, the basal lamina (BL), a layer of the extracellular matrix (ECM) that surrounds the midgut and other major organ systems, represents a barrier to virus spread (Passarelli, 2011), as gaps or pores in the BL are thought to be too small for viral particles to cross (Hess and Falcon, 1987; Reddy and Locke, 1990). Because AcMNPV is found in the caterpillar circulatory system only 30 min postinfection (Granados and Lawler, 1981), the virus must possess mechanisms to rapidly bypass the BL.

An unexplored mechanism for BL penetration is that of BL breakdown using actin-rich podosomes and invadopodia (collectively known as invadosomes) (Linder *et al.*, 2011; Murphy and Courtneidge, 2011). These are dot-like actin-containing structures of 0.5 to 2 μm in diameter (Marchisio *et al.*, 1984; Marchisio, 1987; Tarone *et al.*, 1985; Nermut *et al.*, 1991) that may be organized into dynamic clusters shaped as rings or rosettes (Destaing *et al.*, 2003; Kuo *et al.*, 2018). Invadosomes are characterized by the presence of a dynamic actin core (Destaing *et al.*, 2003) as well as the presence of the actin-associated proteins cortactin (Kanner *et al.*, 1990; Schuuring *et al.*, 1993; Hiura *et al.*, 1995; Oser *et al.*, 2009) and Arp2/3 complex (Linder *et al.*, 1999, 2000; Burns *et al.*, 2001; Yamaguchi *et al.*, 2005), as well as the scaffold protein tyrosine kinase with five SH3 domains (Tks5) (Seals *et al.*, 2005; Di Martino *et al.*, 2014). Invadosomes are also sites of directed ECM degradation by matrix metalloproteases (Chen *et al.*, 1985; Chen, 1989). Invadosomes are common in monocyte-derived cells such as osteoclasts that penetrate the ECM during migration or remodel the ECM (Marchisio *et al.*, 1984; Marchisio, 1987), though they also occur in smooth muscle cells (Hai *et al.*, 2002; Webb *et al.*, 2005; Zhou *et al.*, 2006) and endothelial cells (Moreau *et al.*, 2003; Burgstaller and Gimona, 2005; Varon *et al.*, 2006). Formation of invadosomes is also associated with aggressive cancer cell lines and enables them to remodel the ECM and undergo metastasis (Paz *et al.*, 2014; Eddy *et al.*, 2017). Vertebrate tumor virus infection can also induce invadosome formation. For example, transformation of fibroblasts with Rous sarcoma virus leads to expression of viral-Src (v-Src), a tyrosine kinase that can induce invadosome formation through activation of Tks5 (David-Pfeuty and Singer, 1980; Tarone *et al.*, 1985; Chen, 1989; Seals *et al.*, 2005; Stylli *et al.*, 2009). Whether and how viruses that infect invertebrate animals induce invadopodia has remained uncertain.

Upon investigating AcMNPV-induced cortical actin rearrangements, we found that the virus promotes the formation of actin-containing structures in lepidopteran cells whose appearance and dynamics are similar to those of invadosome clusters in mammalian cells and that serve as sites of ECM degradation. Furthermore, we found that ARIF-1 is necessary and sufficient for the formation of these invadosomes. We mapped the regions of ARIF-1 and identified individual tyrosine and proline residues that are necessary for the formation of invadosome clusters. Finally, we observed that invadosome clusters colocalize with ARIF-1, cortactin, and the Arp2/3 complex and Arp2/3 complex activity is required for their formation and maintenance. Our findings indicate that ARIF-1 induces the formation of invadosomes, which may play a role in accelerating viral infection in insect hosts.

RESULTS

AcMNPV infection induces the formation of dynamic clusters of actin structures

To investigate actin cytoskeleton rearrangements induced by AcMNPV during the early stage of infection, we transiently transfected *Spodoptera frugiperda* Sf21 cells with a plasmid expressing green fluorescent protein (GFP)-tagged actin (GFP-actin) and infected them with AcMNPV. As soon as 3 h postinfection (hpi), cells formed striking actin structures that appeared as small round clusters, circular rosettes, or elongated belts, ranging between 3 and 20 μm in size (Figure 1A). Total internal reflection fluorescence (TIRF) microscopy revealed that these structures were basally located inside the substrate-facing cell surface (Figure 1A). We then quantified the percentage of cells with these actin structures over the course of viral infection. We found that actin structures began to form in cells at 3–4 hpi, were most prevalent between 4 and 8 hpi, and could be found at times as late as 32 hpi (Figure 1B).

To further investigate the dynamics of these structures, we imaged live, infected Sf21 cells from 0 to 8 hpi. We found that the actin structures were highly dynamic in shape and position, could persist for more than 4.5 h, and could undergo fusion or fission events (Figure 1C; Supplemental Video 1). Interestingly, the larger actin structures were clusters made up of many smaller ~0.5 μm dot-like actin puncta (Figure 1C; Supplemental Video 2). Individual actin puncta remained stationary relative to the substrate, and the shape of the cluster changed through appearance or disappearance of individual actin puncta (Figure 1C; Supplemental Video 2). We observed similar dynamic clusters of actin puncta in *B. mori* BmN cells infected with the related baculovirus BmNPV between 6 to 8 hpi (Supplemental Figure S1A; Supplemental Video 3), indicating that this phenomenon is conserved for different baculoviruses and cell types. The appearance and behavior of the actin structures in AcMNPV-infected Sf21 cells and BmNPV-infected BmN cells were also markedly similar to those of invadosome rings and rosettes formed in some mammalian cell types.

To further investigate the kinetics of actin polymerization–depolymerization in these actin structures, we added latrunculin A (latA) to live AcMNPV-infected Sf21 cells and measured their persistence.

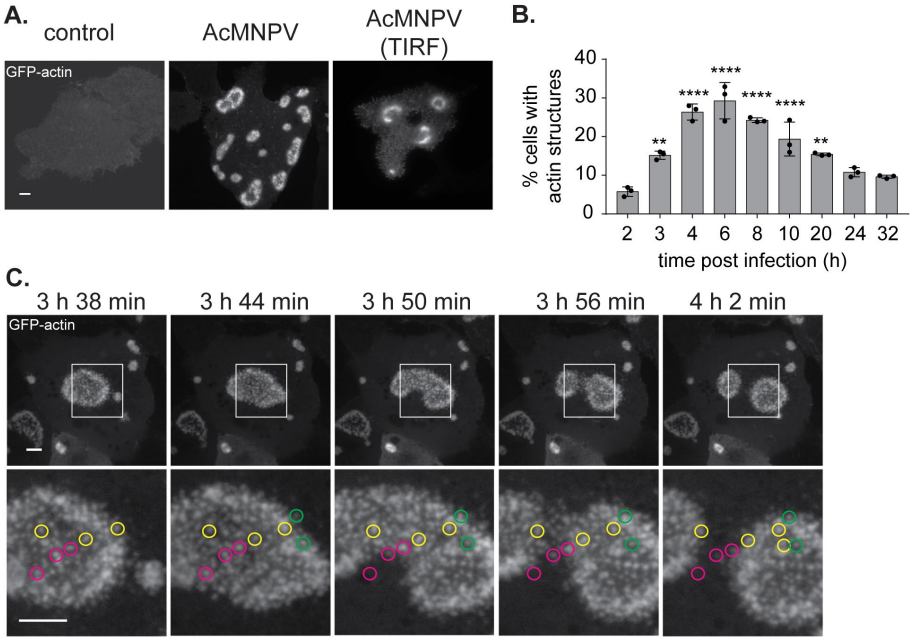

FIGURE 1: Dynamic clusters of actin structures form in Sf21 insect cells during early AcMNPV infection. (A) Confocal and TIRF images of Sf21 insect cells transiently transfected with GFP-actin and mock infected or infected with AcMNPV at an MOI of 10. Images were taken from 4 to 7 hpi. Scale bars = 5 μm. (B) Clusters of actin structures in AcMNPV-infected Sf21 cells were quantified from 2 to 32 hpi. Data are mean ± SD of $n = 3$ biological replicates imaging ~5000 cells each. *P* values were calculated with a one-way analysis of variance (ANOVA) with Tukey's posthoc test relative to the 2 h time point and are indicated as follows: ** = $p < 0.005$, **** = $p < 0.0001$. (C) Confocal time-lapse images of Sf21 insect cells transiently transfected with GFP-actin and infected with AcMNPV. Inset images in the bottom row show red, yellow, and green circles enclosing stationary actin puncta that disappear, are maintained, or appear, respectively. Scale bars = 5 μm. Time postinfection is indicated.

Addition of latA caused the GFP-actin signal in actin structures to rapidly fade with a half-life of ~7–8 min, so that none of the structures remained ~15 min after drug addition (Supplemental Figure S2; Supplemental Video 4). The rapid disappearance of actin structures indicates that actin disassembly in these structures is relatively rapid and that continuous actin polymerization is needed for their assembly and maintenance.

Dynamic clusters of actin structures function as invadosomes in ECM degradation

To determine whether AcMNPV-induced actin structures function as invadosomes, we investigated their ability to degrade an underlying ECM. We plated infected Sf21 cells transiently transfected with GFP-actin onto an ECM substrate consisting of fluorescent fibronectin and simultaneously imaged actin and fibronectin signals. At ~5 hpi, we observed the formation of clusters of actin puncta and the coincident loss of fibronectin signal underneath these structures (Figure 2A). Quantification of actin and fibronectin signal intensities over time at individual clusters of actin puncta revealed a significant inverse correlation, indicating that the appearance of actin structures coincided with loss of fibronectin (Figure 2B). The evidence that loss of fibronectin signal coincides both spatially and temporally with actin structure formation suggests that actin structures direct degradation of underlying ECM. On the basis of the similarities in appearance, dynamics, and ECM degradation activity between actin structures in infected insect cells and invadosomes in mammalian cells, we refer to these virus-induced structures as invadosomes and invadosome clusters.

ARIF-1 is necessary and sufficient for formation of invadosome clusters

We next set out to define the viral gene(s) required for the formation of AcMNPV-induced invadosomes. The AcMNPV *arif-1* gene was previously shown to be necessary and sufficient to induce the accumulation of actin filaments at the cell periphery in TN368 insect cells (Roncarati and Knebel-Mörsdorf, 1997), suggesting that it may be responsible for inducing invadosome formation in Sf21 cells. To determine whether ARIF-1 plays a role in the formation of these structures, we constructed an *AcΔarif-1* virus in the AcMNPV WOBpos background that contained a deletion of 70% of the *arif-1*–coding region (WOBpos is derived from the E2 strain of AcMNPV, and its genome can be propagated as a bacmid in *Escherichia coli* [Goley *et al.*, 2006]). We also constructed an *AcΔarif-1-rescue* virus in which the *arif-1* gene and 500-base-pair flanking regions were inserted at the nearby polyhedrin locus in the *AcΔarif-1* viral genome. Sf21 cells infected with *AcΔarif-1* completely lacked invadosome clusters (Figure 3, A and B). The formation of invadosome clusters was fully restored in cells infected with the *AcΔarif-1-rescue* virus (Figure 3, A and B). This demonstrates that ARIF-1 is necessary for invadosome cluster formation in infected Sf21 cells.

To determine whether ARIF-1 is sufficient for invadosome cluster formation, we transiently transfected Sf21 cells with plasmid pACT-*arif-1*, which included *arif-1* under the control of the *B. mori* actin promoter. Transfected Sf21 cells formed invadosome clusters (Figure 3, C and D) that maintained a variety of shapes similar to those in infected cells (small and round, circular rosettes, or elongated belts). The dynamic behavior of these structures was also similar to that in infected cells (Supplemental Video 5). Overall, these data indicate that the expression of *arif-1* alone is sufficient for the formation of invadosome clusters in Sf21 cells.

To verify that the timing of ARIF-1 expression and invadosome cluster formation were consistent with one another, we raised a polyclonal ARIF-1 antibody and probed lysates of cells infected with AcMNPV, *AcΔarif-1*, and *AcΔarif-1-rescue* viruses over a time course of infection (Supplemental Figure S3). ARIF-1 was expressed in cells infected with wild-type and *AcΔarif-1-rescue* viruses but absent from cells infected with *AcΔarif-1*. Furthermore, the timing of ARIF-1 expression was consistent with the timing of invadosome formation and disappearance (Figure 1B; Supplemental Figure S3). This confirms that invadosome formation is correlated with ARIF-1 expression.

ARIF-1 is localized to invadosome clusters

ARIF-1 was previously reported to exhibit general localization to the plasma membrane in TN368 cells (Dreschers *et al.*, 2001). To determine whether ARIF-1 concentrates in invadosome clusters, we investigated the localization of both endogenous ARIF-1 and transiently transfected GFP-tagged ARIF-1 (GFP-ARIF-1) in Sf21 cells. We first used immunofluorescence microscopy to visualize endogenous ARIF-1 in Sf21 cells infected with AcMNPV, *AcΔarif-1*, or *AcΔarif-1-rescue* virus at 5 hpi (Figure 4A). Endogenous ARIF-1 was

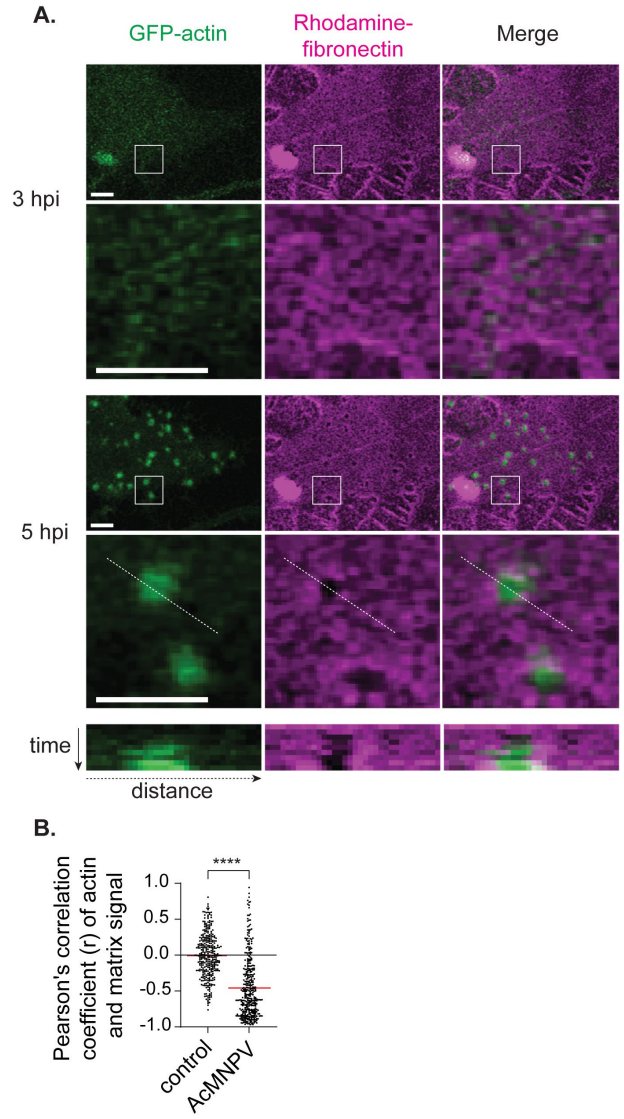

FIGURE 2: AcMNPV-induced invadosomes degrade underlying extracellular matrix. (A) Images of Sf21 cells plated on rhodamine-fibronectin matrix, transiently transfected with GFP-actin, infected with an AcMNPV MOI of 10, and imaged at 3 and 5 hpi. Insets at 5 hpi show areas where invadosome clusters correspond with areas of cleared matrix. The white dotted line was used to make a kymograph showing GFP-actin accumulation and matrix clearing over time. Scale bars = 5 μm. (B) Quantification of Pearson's correlation coefficients of GFP-actin and matrix signal intensities measured over 2 h in cells infected with AcMNPV or mock infected (control). Intensities of actin and matrix signals were measured at the site of invadosome clusters in AcMNPV-infected cells or at random sites in mock infected cells. Negative values indicate an inverse correlation between GFP-actin signal and matrix signal intensity at a single site. Data represent individual measured sites and were taken from $n = 3$ biological replicates of 11 cells for each treatment. The p value was calculated by an unpaired t test; **** = $p < 0.0001$.

concentrated at invadosome clusters in cells infected with AcMNPV and *AcΔarif-1-rescue* viruses but was absent in mock-infected and *AcΔarif-1* virus–infected cells (Figure 4A). To determine whether ARIF-1 also localizes to invadosome clusters in uninfected cells, we transiently transfected Sf21 cells with plasmids expressing GFP-ARIF-1 and the filamentous actin probe F-tractin tagged with mCherry (F-tractin-mCherry) (Figure 4B). In these transiently transfected cells, GFP-ARIF-1 localized to invadosome clusters labeled with F-tractin-mCherry (Figure 4B). Thus, ARIF-1 is enriched at invadosome clusters in both infected and ARIF-1–expressing cells.

The ARIF-1 C-terminal region is necessary and sufficient for invadosome cluster formation

Prior structural predictions and our own analyses suggested that ARIF-1 contains three N-terminal transmembrane domains and a ~200-amino-acid (aa) C-terminal region that extends into the cytoplasm (Dreschers *et al.*, 2001) (Figure 5A). We first sought to determine which parts of the ARIF-1 C-terminal region are necessary for the formation of clusters of invadosomes. We constructed a series of C-terminal truncations of ARIF-1 and quantified the formation of invadosome clusters in transiently transfected Sf21 cells (Figure 5B and Supplemental Figure S4A). Although expression of ARIF-1(1–401) (containing C-terminal residues up through aa 401), ARIF-1(1–398), ARIF-1(1–378), and ARIF-1(1–371) caused a reduced percentage of cells with invadosome clusters when compared with expression of the full-length protein ARIF-1(1–417), these clusters still formed. However, no such structures formed in cells transfected with ARIF-1(1–274). This indicates that the ARIF-1 C-terminus between residues 274 and 371 is necessary for the formation of invadosome clusters.

To determine the contributions of the ARIF-1 N-terminal and transmembrane regions, we transfected cells with a plasmid that expressed ARIF-1(219–417) missing N-terminal aa 1–218 that encode the predicted transmembrane domains and cytoplasmic loop (Figure 5C). Sf21 cells transiently transfected with ARIF-1(219–417) did not form invadosome clusters (Figure 5C and Supplemental Figure S4B), indicating that the transmembrane domains are required for ARIF-1 function. Next, to test whether membrane targeting of the C-terminus is sufficient for the formation of invadosome clusters, we expressed a variant of ARIF-1 in which the ARIF-1 C-terminus was fused to the unrelated AcMNPV transmembrane protein GP64 (Figure 5A, right). Surprisingly, a similar percentage of cells expressing GP64::ARIF-1(219–417) formed invadosome clusters compared with cells expressing full-length ARIF-1(1–417) (Figure 5C and Supplemental Figure S4B; Supplemental Video 6). This indicates that the membrane-targeted ARIF-1 C-terminus from residues 219–417 is sufficient for the formation of clusters of invadosomes and that the ARIF-1 N-terminal cytoplasmic loop and transmembrane regions function to anchor the ARIF-1 C-terminal region to the plasma membrane.

To further narrow down which regions of the ARIF-1 C-terminus are necessary for the formation of invadosome clusters, we constructed a series of N-terminal truncations to GP64::ARIF-1(219–417) and quantified invadosome formation in transiently transfected Sf21 cells. Cells expressing GP64::ARIF-1(274–417) and GP64::ARIF-1(303–417) had invadosome clusters, whereas these structures were completely absent in cells expressing GP64::ARIF-1(320–417) (Figure 5C and Supplemental Figure S4B). Altogether, the data from the expression of various truncation derivatives indicate that the ARIF-1 C-terminus between residues 303 and 371 is necessary for the formation of invadosome clusters.

ARIF-1 residues Y332F and P335A are important for invadosome cluster formation

We next sought to identify individual residues in the ARIF-1 C-terminal region that may be important for the formation of invadosome clusters. ARIF-1 is tyrosine-phosphorylated during infection, though which tyrosine residues are phosphorylated is unknown (Dreschers *et al.*, 2001). The ARIF-1 C-terminus also contains several stretches rich in proline residues (Figure 6A). We sought to assess the

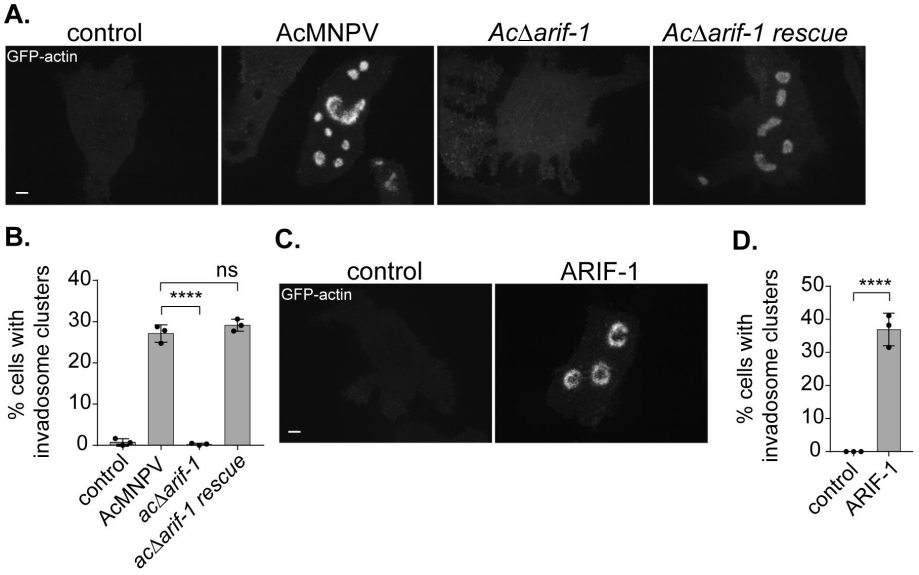

FIGURE 3: ARIF-1 is necessary and sufficient for the formation of invadosome clusters. (A) Confocal images of Sf21 cells transiently transfected with GFP-actin and infected with an MOI of 10 of the indicated virus. Images were taken at 4 hpi and are representative of three biological replicates. Scale bars = 5 μm. (B) Clusters of invadosomes in infected cells were quantified at 4 hpi. Data are mean ± SD of $n = 3$ biological replicates of ~5000 cells each. *P* values were calculated by one-way ANOVA with multiple comparisons and are indicated as follows: ns = not significant, **** = $p < 0.0001$. (C) Images of Sf21 cells transiently expressing GFP-actin and ARIF-1. Images were taken 2 d posttransfection and are representative of three biological replicates. Scale bars = 5 μm. (D) Quantification of invadosome clusters in cells transfected with GFP-actin and ARIF-1. Structures were quantified by eye 2 d posttransfection. Data are mean ± SD of $n = 3$ biological replicates of 60 cells each treatment. The *p* value was calculated by an unpaired *t* test; **** = $p = 0.0002$.

importance of individual tyrosine and proline residues by mutating tyrosine to phenylalanine and proline to alanine (Figure 6A). We then quantified invadosome clusters in Sf21 cells transiently expressing ARIF-1 mutants (Figure 6, B and C). While most mutations did not significantly affect the formation of invadosome clusters, cells transiently transfected with ARIF-1(Y332F) and ARIF-1(P335F) mutations had no clusters but formed invadosomes uniformly dispersed across the basal cell surface (Figure 6D and Supplemental Figure S5, A and B; Supplemental Videos 7 and 8). Mutations in BmNPV ARIF-1 analogous to AcMNPV ARIF-1 Y332F and P335A recapitulated the uniform invadosome dispersal phenotype in transiently transfected cells (Supplemental Figure S1B). To verify that differences in the formation of invadosomes clusters in ARIF-1 tyrosine and proline point mutants were not due to differences in expression levels of the ARIF-1 point mutant, we probed cell lysates using the ARIF-1 antibody (Supplemental Figure S6, A and B). ARIF-1 was detected in cells transfected with ARIF-1 Y332F and P335A mutations, demonstrating that the lack of invadosome clusters was not due to decreased ARIF-1 expression. Our results are consistent with truncation analyses, which pointed to key residues between AcMNPV ARIF-1 303–371 and suggest that adjacent residues Y332 and P335 facilitate the formation of clusters of invadosomes.

Cortactin and the Arp2/3 complex play a role in the formation and maintenance of invadosome clusters

The actin core of podosomes in mammalian cells includes cortactin (Schuuring *et al.*, 1993; Hiura *et al.*, 1995) and the Arp2/3 complex (Linder *et al.*, 1999, 2000; Mizutani *et al.*, 2002). To determine whether invadosomes in lepidopteran cells have a similar protein composition, we investigated whether cortactin and the Arp2/3 complex colocalize with these structures. GFP-tagged *S. frugiperda* cortactin (GFP-cortactin) was expressed in Sf21 cells by transient transfection, and cells were subsequently infected with AcMNPV and imaged at 4 hpi. GFP-cortactin colocalized with actin in invadosome clusters (Figure 7A). To determine whether the Arp2/3 complex localizes to invadosome clusters, we expressed GFP-tagged Arp2/3 complex subunit ARPC3 (GFP-ARPC3) in Sf21 cells by transient transfection and similarly infected these cells with AcMNPV and imaged at 4 hpi. GFP-ARPC3 also colocalized with invadosome clusters (Figure 7B). Thus, both cortactin and the Arp2/3 complex are present at these areas of dynamic actin polymerization.

To determine whether the host Arp2/3 complex plays a role in the formation and maintenance of invadosomes, we treated infected cells with Arp2/3 complex inhibitor CK666 or with the inactive control drug CK689. Invadosome clusters were virtually eliminated 1 h posttreatment with Arp2/3 inhibitor CK666, but no significant effect was observed upon treatment with CK689 (Figure 7C; Supplemental Videos 9 and 10). Thus, host Arp2/3 complex function is required for the formation and maintenance of these structures.

DISCUSSION

Here, we describe the formation of dynamic actin structures in AcMNPV-infected lepidopteran insect cells that coalesce into clusters, rosettes, and rings and that degrade underlying ECM, resembling invadosome clusters in mammalian cells. We further show that the AcMNPV protein ARIF-1 is necessary and sufficient for the formation of these invadosome clusters. We identify regions of ARIF-1 and individual proline and tyrosine residues critical for their formation. Finally, we verify that ARIF-1, cortactin, and the Arp2/3 complex localize with invadosome clusters and that Arp2/3 complex function is important for their maintenance. Our results indicate that ARIF-1 induces the formation of invadosomes in lepidopteran cells and that these structures may facilitate systemic AcMNPV spread in hosts.

Our results add to previous observations by describing the formation of AcMNPV-induced and ARIF-1–dependent invadosomes. Previously, it was noted that during early-stage AcMNPV infection, actin accumulated evenly around the periphery of TN368 and BmN cells (Roncarati and Knebel-Mörsdorf, 1997; Kokusho *et al.*, 2015) and accumulated in "ventral aggregates" at the basal cell surface in Sf21 cells (Charlton and Volkman, 1991). However, the finer organization and dynamics of this peripheral actin was not described. Using live cell imaging, we observed that ARIF-1 induces the formation of actin puncta that cluster together into dynamic clumps, rosettes, or belts and that these can persist for hours and change shape and position. Though we were unable to observe invadosome clusters or peripheral actin accumulation in TN368 cells, we and others observe invadosome clusters in AcMNPV-infected Sf21 cells (Charlton and Volkman, 1991) and Sf9 cells (unpublished data), as

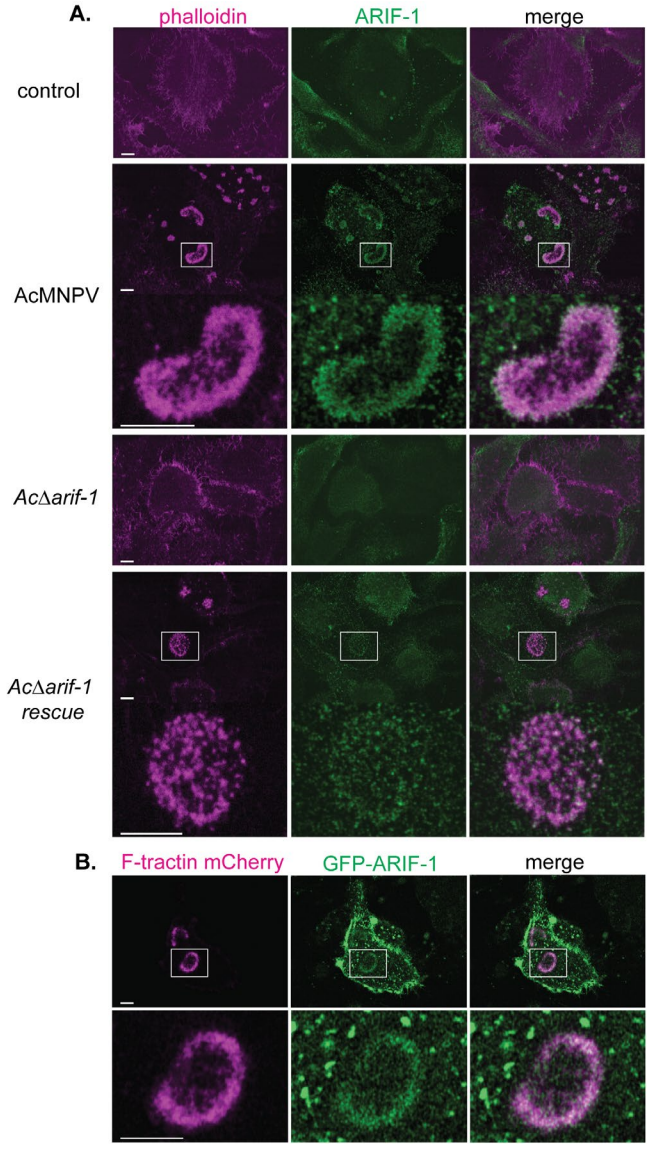

FIGURE 4: ARIF-1 colocalizes with invadosome clusters. (A) Confocal immunofluorescence microscopy images of Sf21 cells infected with the indicated virus. Cells were fixed at 5 hpi and stained with anti–ARIF-1 antibody and fluorescent phalloidin. Insets show selected invadosome clusters. Scale bars = 5 μm. (B) Confocal images of live Sf21 cells transiently expressing F-tractin-mCherry and GFP-ARIF-1. Images were taken 2 d postransfection. Insets show selected invadosome clusters. Scale bars = 5 μm.

well as BmNPV-infected BmN cells, indicating that the induction of these structures is conserved between different baculoviruses and cell lines.

ARIF-1–induced actin structures in Sf21 cells are similar to podosomes and invadopodia in appearance and dynamics. In mammalian osteoclasts, many stationary dot-like podosomes organize into clusters that merge to form one large ring around the cell periphery (Destaing *et al.*, 2003; Luxenburg *et al.*, 2007). The shape of these ring structures is determined by selective activation and inactivation of stationary podosomes (Destaing *et al.*, 2003) in the same way that individual pixels on a screen turn on or off to create a moving image. We have observed a similar phenomenon in invadosome clusters in AcMNPV-infected or *arif-1*–transfected Sf21 cells. However, instead of full podosome rings as seen in osteoclasts, these structures more closely resemble invadopodia rosettes in v-Src–transformed fibroblast cells (Tarone *et al.*, 1985). Intriguingly, invadopodia rosettes have also been described as dynamically changing shape (Stickel and Wang, 1987), fusing together (Kuo *et al.*, 2018), or splitting in two to form new invadopodia rosettes (Kuo *et al.*, 2018), all of which we also observed in invadosome clusters in lepidopteran cells. Individual osteoclast podosomes persist for 2 min on average, with actin turning over approximately every 1 min (Destaing *et al.*, 2003). Meanwhile, podosome clusters in these cells persist for several hours (Destaing *et al.*, 2003). In lepidopteran cells, our results suggest that actin in invadosomes has a half-life of ~7 min and clusters persist for hours.

ARIF-1–induced invadosomes are also similar to podosomes and invadopodia in terms of their ability to degrade underlying ECM. Podosomes and invadopodia recruit and activate zinc-regulated matrix metalloproteases (MMPs) (Linder *et al.*, 2011; Murphy and Courtneidge, 2011; Castro-Castro *et al.*, 2016), ADAM family proteases (Abram *et al.*, 2003), membrane-bound serine proteases (Monsky *et al.*, 1994; Mueller *et al.*, 1999), and cathepsin cysteine proteases (Tu *et al.*, 2008) to mediate degradation of ECM components, including type I and IV collagen, laminin, and fibronectin (Kelly *et al.*, 1994; Murphy and Courtneidge, 2011). Our observation of temporal and spatial colocalization of clusters of actin structures with focal degradation of fibronectin matrix in AcMNPV-infected insect cells suggests that these ARIF-1–induced structures function as invadosomes by directing degradation of the ECM. Although betabaculovirus genomes encode a viral MMP (Ishimwe *et al.*, 2016), all alphabaculoviruses including AcMNPV lack a gene encoding a viral MMP. Instead, AcMNPV expresses a viral fibroblast growth factor (vFGF) in infected cells (Katsuma *et al.*, 2004) that is secreted (Katsuma *et al.*, 2004; Detvisitsakun *et al.*, 2005; Lehiy *et al.*, 2009) and binds to insect FGF receptors (Katsuma *et al.*, 2006). vFGF-mediated signaling induces cleavage and activation of an MMP-9 orthologue, which activates effector caspases that degrade the ECM and remodel the insect BL (Means and Passarelli, 2010; Passarelli, 2011). Deletion of the *vfgf* gene from AcMNPV delays the dissemination of AcMNPV from the site of initial infection, leading to a delay in host insect death (Detvisitsakun *et al.*, 2007; Means and Passarelli, 2010), similar to the effect of *arif-1* deletion (Kokusho *et al.*, 2015). The similar effects of baculovirus *arif-1* and *vfgf* deletions on host insect mortality coupled with the effects of vFGF on BL remodeling and ARIF-1 on matrix degradation suggest that ARIF-1 may act in concert with vFGF and other viral proteins to remodel the insect BL by inducing the formation of invadosomes that may direct vFGF-activated MMP and caspase activity.

ARIF-1–induced invadosomes contain proteins that play key roles in the formation and maintenance of podosomes and invadopodia in mammalian cells. We confirmed that ARIF-1 localizes to the plasma membrane, colocalizing with actin in invadosome clusters. Furthermore, actin, cortactin, and the Arp2/3 complex localize to invadosomes themselves. These are also critical components of mammalian podosomes and invadopodia (Kanner *et al.*, 1990; Schuuring *et al.*, 1993; Hiura *et al.*, 1995; Linder *et al.*, 1999, 2000; Burns *et al.*, 2001; Destaing *et al.*, 2003; Yamaguchi *et al.*, 2005; Oser *et al.*, 2009), implying a parallel between invadosomes in mammalian and lepidopteran cells. Interestingly, the scaffolding protein Tks5, which is a distinct marker of podosomes and invadopodia in mammalian cell types (Seals *et al.*, 2005; Stylli *et al.*, 2009; Burger *et al.*, 2014; Di Martino *et al.*, 2014), lacks a clear orthologue in *S. frugiperda*. This suggests the possibility that ARIF-1 itself may be acting as a scaffolding protein, playing a role similar to that of mammalian Tks5 in invadosome assembly.

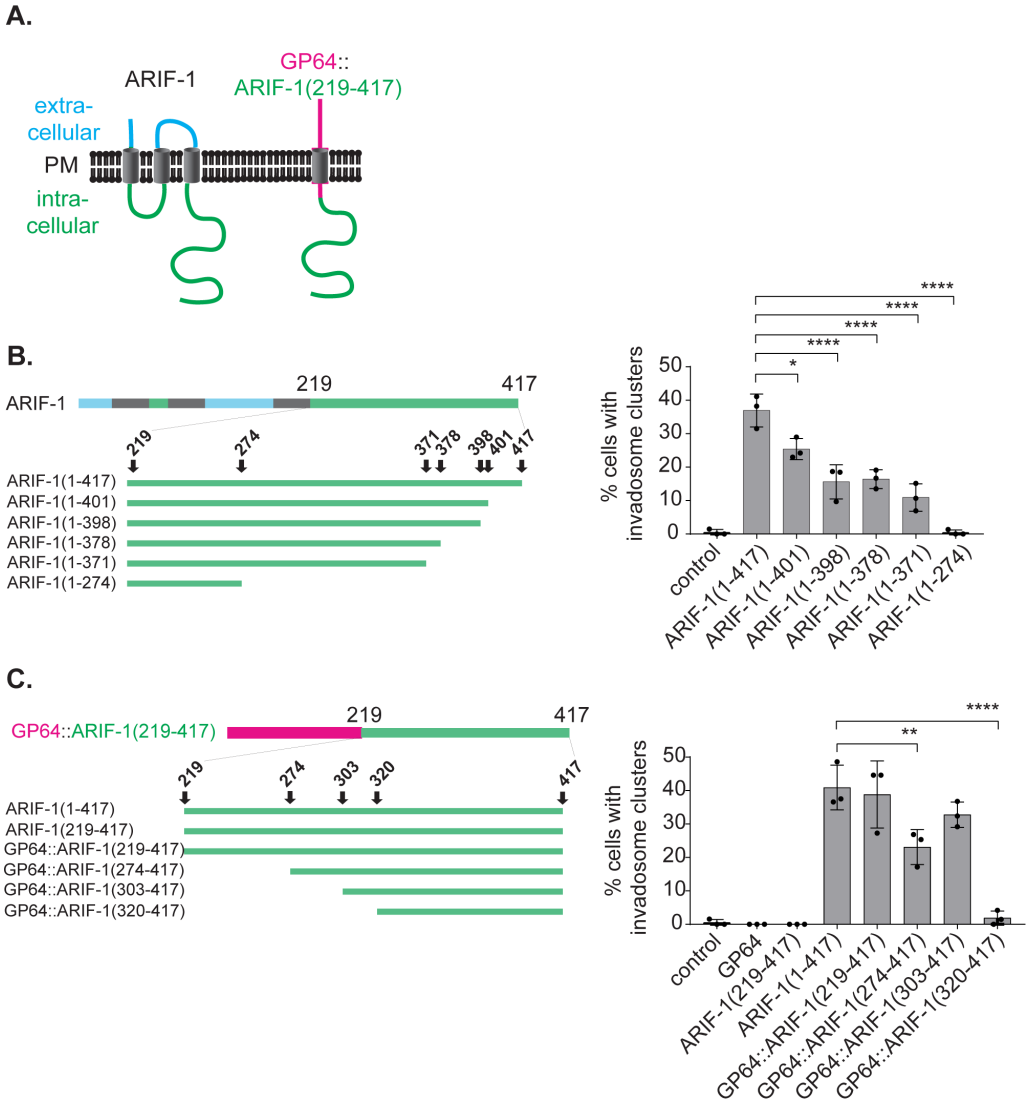

FIGURE 5: ARIF-1 residues 303–371 are necessary for the formation of invadosome clusters. (A) Left: predicted ARIF-1 structure with three transmembrane domains and a cytoplasmic C-terminal region (aa 219–417). Right: AcMNPV transmembrane protein GP64 (red) fusion to ARIF-1 C-terminal region. (B) Left: visual representation of ARIF-1 C-terminal truncations. Right: quantification of invadosome clusters in Sf21 cells transiently expressing GFP-actin and truncated ARIF-1 2 d posttransfection. Data are mean ± SD of $n = 3$ biological replicates of 60 cells each. *P* values were calculated with a one-way ANOVA with multiple comparisons, comparing each treatment to ARIF-1 (1–417), and are indicated as follows: * = $p = 0.0167$, **** = $p < 0.0001$. (C) Left: visual representation of AcMNPV transmembrane protein GP64 (red) fused to ARIF-1(219–417) and N-terminal truncations. Right: quantification of invadosome clusters in Sf21 cells transiently expressing GFP-actin and the indicated construct 2 d posttransfection. Data are mean ± SD of $n = 3$ biological replicates of 60 cells each. *P* values were calculated with a one-way ANOVA with multiple comparisons, comparing each treatment to ARIF-1 (1–417), and are indicated as follows: ** = $p = 0.0075$, **** = $p < 0.0001$.

We identified sequences in the ARIF-1 C-terminal region as well as specific residues that are required for forming clusters of invadosomes. While the ARIF-1 C-terminus from aa 303–371 is required for the formation of clusters of invadosomes, residues Y332 and P335 are required for cluster formation. In cells expressing AcMNPV ARIF-1 with Y332F and P335A point mutations, as well as BmNPV ARIF-1 with analogous Y335F and P338A point mutations, invadosomes were distributed across the entire basal plasma membrane rather than in defined clusters. That a phosphoablative tyrosine-to-phenylalanine mutation at residue 332 causes this phenotype suggests that Y332 may be phosphorylated. Phosphorylated tyrosine residues are key components of binding sites for Src homology 2 (SH2) domains (Buday *et al.*, 2002; Filippakopoulos *et al.*, 2009), which are common in proteins such as Grb-2 and Nck-1 that regulate actin cytoskeleton activity. A truncated ARIF-1 (ARIF-1(1–255)) is also tyrosine-phosphorylated during infection (Dreschers *et al.*, 2001), indicating that additional ARIF-1 tyrosine residues are likely phosphorylated. Increased ARIF-1 phosphorylation as infection progresses was speculated to be correlated with the disappearance of the ARIF-1–induced peripheral actin in TN368 cells (Dreschers *et al.*, 2001). Thus, ARIF-1 tyrosine phosphorylation at Y332 may play a role during early AcMNPV infection, possibly by generating a binding site for cellular or viral proteins that regulate actin polymerization in invadosomes, leading to formation of organized clusters.

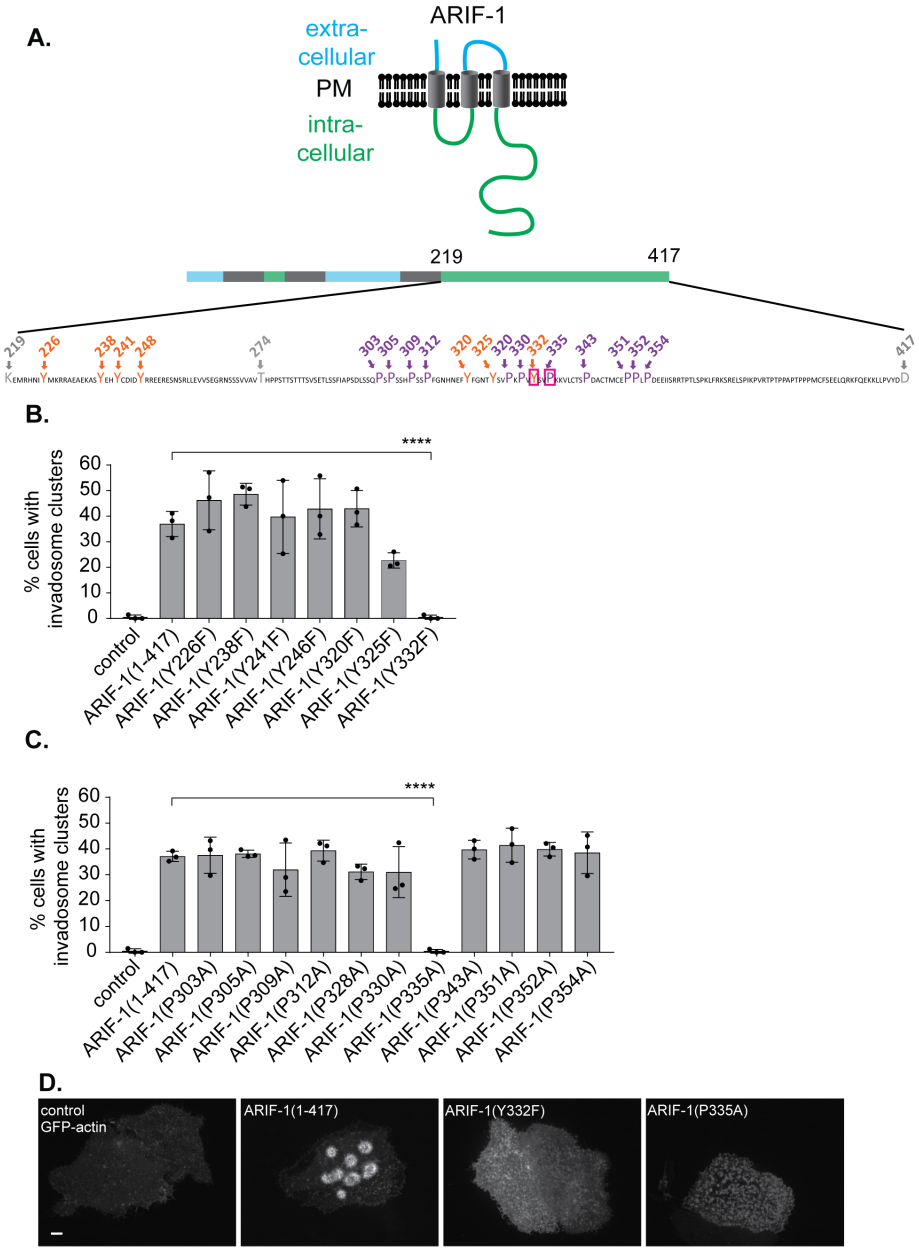

FIGURE 6: ARIF-1 residues Y332F and P335A are important for the formation of invadosome clusters. (A) Tyrosine (Y, orange) and proline (P, purple) residues are indicated on the C-terminal region of ARIF-1. (B) Invadosome clusters in cells transiently transfected with GFP-actin and the indicated tyrosine-to-phenylalanine point mutations were quantified 2 d posttransfection. Data are mean ± SD of $n = 3$ biological replicates of 60 cells each. *P* values were calculated with a one-way ANOVA with multiple comparisons, comparing each treatment to ARIF-1 (1–417), and are indicated as follows **** = $p < 0.0001$. (C) Invadosome clusters in cells transiently transfected with GFP-actin and the indicated proline-to-alanine point mutations were quantified 2 d posttransfection. Data are mean ± SD of $n = 3$ biological replicates of 60 cells each. *P* values were calculated with a one-way ANOVA with multiple comparisons, comparing each treatment to ARIF-1 (1–417), and are indicated as follows: **** = $p < 0.0001$. (D) Confocal images of Sf21 cells transiently expressing GFP-actin and the indicated ARIF-1 mutation. Images are representative of three biological replicates. Scale bars = 5 μm.

Our findings describe ARIF-1–induced invadosome clusters in insect cells. At the level of the host caterpillar, ARIF-1 has also been shown to play a role in viral spread (Kokusho *et al.*, 2015). One explanation that could link the cellular-level and organismal-level functions of ARIF-1 is that ARIF-1–induced invadosomes might mediate degradation of the underlying ECM and degrade barriers to viral infection, such as the insect BL. This hypothesis may inform current models of how other viruses, including human arbovirus pathogens, cross the BL in their insect hosts. For example, eastern equine encephalitis virus disrupts the midgut BL of infected mosquitoes (Weaver *et al.*, 1988), though the mechanism of this disruption is unknown. While invadosome formation has not previously been described in lepidopteran cell lines, invadosome-like structures have been described playing a role in myoblast fusion in *Drosophila*, though these structures were not organized into larger clusters (Onel and Renkawitz-Pohl, 2009; Sens *et al.*, 2010; Haralalka *et al.*, 2011). Such insect invadosomes may hint at the existence of an ancestral podosome or invadopodium activation pathway retained by both mammalian and invertebrate animals that may be taken advantage of by viral pathogens. Thus, further understanding of the molecular mechanisms of podosome and invadopodia formation in both mammalian and insect cell models may uncover conserved roles in infection and other diseases.

MATERIALS AND METHODS

Request a protocol through *Bio-protocol*.

Cell lines and viruses

S. frugiperda ovarian-derived Sf9 cells were maintained in suspension culture in ESF 921 media (Expression Systems; 96-001-01) and in adherent culture in Grace's media (Gemini Bio-Products; 600-310) with 10% fetal bovine serum (FBS; Gemini Bio-Products; 100-500) on T-25 tissue culture flasks at 28°C. *S. frugiperda* ovarian-derived Sf21 cells were maintained in suspension culture in Grace's media with 10% FBS and 0.1% pluronic F-68 (Life Technologies from Thermo Fisher Scientific; 24040032) at 28°C, and in adherent culture on T-25 tissue culture flasks in Grace's media with 10% FBS at 28°C. *B. mori* ovarian-derived BmN cells were a generous gift from Kostas Iatrou (Institute of Biosciences & Applications, National Centre for Scientific Research, Greece) through Don Jarvis (University of Wyoming). These cells were maintained in adherent culture on T-25 tissue culture flasks in TC-100 media (Life Technologies from Thermo Fisher Scientific; 13055025) with 10% FBS (Gemini Bio-Products) at 28°C. BmNPV virus (T3) was a generous gift from Masashi Iwanaga (Utsunomiya University, Japan). *Trichoplusia ni* ovarian-derived TN368 cells were a generous gift from Bob Harrison (Invasive Insect Biocontrol & Behavior Laboratory, Beltsville, MD) and were maintained in adherent culture on T-25 tissue culture flasks in TNMFH

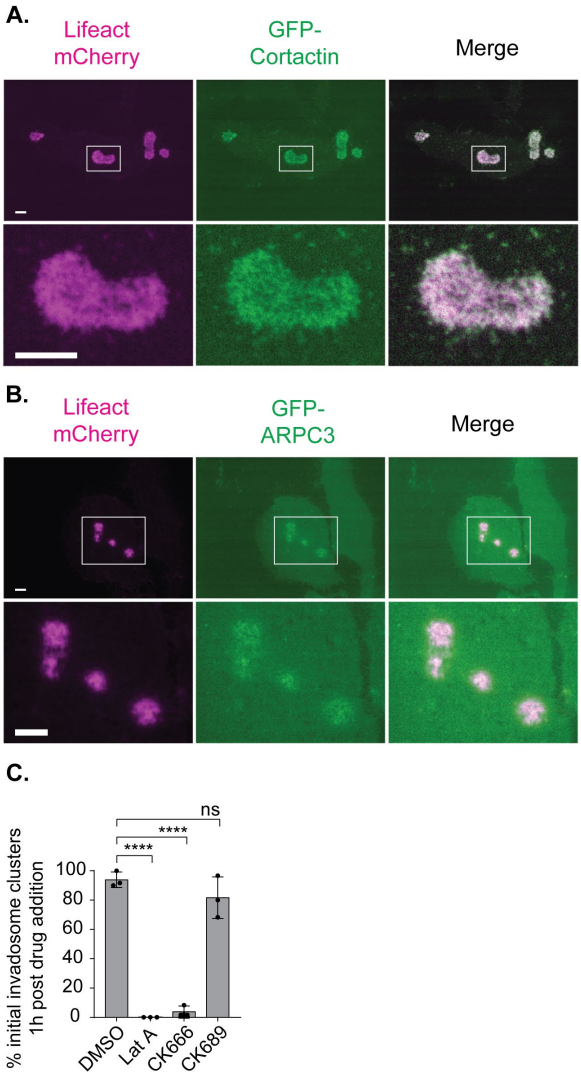

FIGURE 7: Cortactin and the Arp2/3 complex are present at invadosome clusters, and Arp2/3 complex is required for their formation and maintenance. (A) Confocal images of Sf21 cells transiently expressing Lifeact mCherry and GFP-tagged *S. frugiperda* cortactin. Images were taken 2 d posttransfection and are representative of three biological replicates. Scale bars = 5 µm. (B) Confocal images of Sf21 cells transiently expressing Lifeact mCherry and GFP-tagged Arp2/3 complex subunit ARPC3. Images were taken 2 d posttransfection and are representative of three biological replicates. Scale bars = 5 µm. (C) Invadosome clusters were quantified 1 h after the indicated drugs were added to Sf21 cells infected with an AcMNPV MOI of 10 at 4 hpi. Data are mean ± SD of $n = 3$ biological replicates of 40 invadosome clusters. *P* values were calculated with a one-way ANOVA with multiple comparisons, comparing each treatment to ARIF-1 (1–417), and are indicated as follows: ns = not significant, **** = $p < 0.0001$.

media (Gemini Bio-Products; 600-311) with 10% FBS (Gemini Bio-Products) at 28°C. AcMNPV WOBpos (Goley *et al.*, 2006), derived from AcMNPV E2, was used as the wild-type virus.

Generation of recombinant viruses

To generate AcMNPV lacking a functional *arif-1* gene (*AcΔarif-1*), we constructed a transfer vector by subcloning a *Sal*I/*Xho*I fragment of AcMNPV viral genomic fragment EcoRI A, which contains *arif-1*, into the *Xho*I site of pBluescript II SK+ (Addgene) to create the plasmid pEcoRI_ASalxh.pBSKS.rev. This plasmid was digested with *Mlu*I (New England Biolabs), removing 74% of the *arif-1*–coding region, which was replaced with a subcloned 5.4 kb fragment of pBlue-Tet, containing *lacZ* and tetracycline-resistance (*tetR*) genes (Ohkawa *et al.*, 2005; Goley *et al.*, 2006) to help in the selection of recombinant bacmids. The transfer vector was linearized by digestion with *Sma*I and *Apa*I (New England Biolabs) and purified by agarose gel electrophoresis. DNA (30 fmol) was coelectroporated with 0.2 µg of WOBpos bacmid DNA (containing the kanamycin-resistance [*kanR*] gene) into BW251143/pKD46 *E. coli* (Datsenko and Wanner, 2000), which expresses an arabinose-inducible recombinase on a plasmid with temperature-sensitive replication (Goley *et al.*, 2006). Recombinant bacmids were selected by plating on Luria–Bertani (LB) agar plates with 50 µg/ml kanamycin (Life Technologies from Thermo Fisher Scientific) and 10 µg/ml tetracycline (MilliporeSigma).

To generate an *AcΔarif-1* rescue virus (*AcΔarif-1-rescue*), we introduced the *arif-1* gene into the polyhedrin locus of the *AcΔarif-1* bacmid. To do this, we generated the transfer plasmid pARIF-1-Rescue-2 by PCR, amplifying a 2.2 kb fragment including *arif-1* and 500-base-pair 5′ and 3′ flanking sequences from pEcoRI_ASalxh.pBSKS.rev and inserted it using Gibson assembly (New England Biolabs; Gibson *et al.*, 2009) into pWOBCAT (Ohkawa *et al.*, 2010) amplified and linearized by PCR, inserting it upstream of a chloramphenicol resistance (*cat)* gene to help in the selection of recombinant bacmids. The resulting plasmid was digested with *Not*I and *Kas*I (New England Biolabs) to remove a truncated *kanR* gene upstream of *arif-1*, which was replaced by ligating (Takara Bio USA) a 2 kb PCR-amplified fragment from pWOBpos2 (Goley *et al.*, 2006) including the AcMNPV mini–F replicon and a full *kanR* gene in place of the truncated *kanR* gene. This plasmid transfer vector, pARIF-1-Rescue-2, was linearized through *Kpn*I digestion (New England Biolabs) and purified by agarose gel electrophoresis. DNA (30 fmol) was electroporated with 0.2 µg of *AcΔarif-1* bacmid DNA into BW251143/pKD46 *E. coli* as described above, and bacteria were plated on LB agar plates with 25 µg/ml chloramphenicol and 10 µg/ml tetracycline (MilliporeSigma).

In all cases, positive colonies were grown in 2× YT media (MilliporeSigma) with 25 µg/ml kanamycin (Life Technologies from Thermo Fisher Scientific) for 18 h at 37°C. Bacmid DNA was extracted and transfected into Sf9 cells using TransIT-Insect Transfection reagent (Mirius Bio; MIR6100). The resulting virus was amplified by passaging in Sf9 cells and correct homologous recombination verified through restriction enzyme digestion of viral DNA. PCR and sequencing of viral DNA was also used to confirm the presence of each desired genome modification.

Plasmid construction for expression of wild-type and mutant ARIF-1

To express full-length ARIF-1 and ARIF-1 C-terminal truncations, we used PCR to amplify the following AcMNPV *arif-1* regions from pEcoRI_ASalxh.pBSKS.rev (listed as aa numbers): ARIF-1(1–417), ARIF-1(1–219), ARIF-1(1–274), ARIF-1(1–371), ARIF-1(1–378), ARIF-1(1–398), and ARIF-1(1–401) along with C-terminal TAG stop codons. Fragments were purified by agarose gel electrophoresis and individually subcloned into *Bam*HI/*Not*I-digested pBluescript II KS+ (Addgene). Colonies positive for the plasmid were selected on LB agar with 100 µg/ml ampicillin (Life Technologies from Thermo Fisher Scientific), 100 µM 5-bromo-4-chloro-3-indolyl-β-D-galactopyranoside (X-Gal), and 100 µM isopropyl β-D-1-thiogalactopyranoside (IPTG). Next, these plasmids were digested with *Bam*HI and *Not*I (New England Biolabs) and subcloned into *Bam*HI/*Not*I-digested pACT

(Ohkawa *et al.*, 2002). The resulting plasmids have a *B. mori* actin promoter driving expression of each ARIF-1 truncation.

To generate ARIF-1 C-terminally tagged with eGFP-FLAG as well as GlyGlyGlyGlySer-eGFP-FLAG (with a N-terminal linker), we amplified two DNA fragments with PCR and used Gibson assembly to subclone these into the *Bam*HI site of pBluescript II KS+ (Addgene). The first fragment, containing *arif-1,* was amplified from pEcoRI_ASalxh.pBSKS.rev with reverse primers incorporating or not incorporating a C-terminal GlyGlyGlyGlySer linker. The second fragment, containing *eGFP,* was amplified from pEGFP-N1 (Takara Bio USA) with the reverse primer incorporating a FLAG tag. Colonies positive for the assembled plasmid were selected on LB agar with 100 μg/ml ampicillin, 0.1 mM X-Gal, and 40 μg/ml IPTG. We then PCR-amplified the ARIF-1-eGFP-FLAG or ARIF-1-GlyGlyGlyGlySer-eGFP-FLAG sequence and used Gibson assembly to subclone it into the *Not*I site of pACT.

To generate fusions of ARIF-1 and its N-terminal truncations to AcMNPV GP64, we PCR-amplified two fragments and assembled them into the *Not*I site of pACT. The first fragment was *gp64* from the 14 kb viral fragment XhoI G. The second fragment was amplified from pEcoRI_ASalxh.pBSKS.rev and encoded one of the following regions of *arif-1* (listed as aa numbers): K219–D417, T274–D417, P303–D417, or Y320–D417. The resulting plasmids encode ARIF-1 and its truncations fused to the C-terminus of GP64.

To express ARIF-1 with point mutations of proline and tyrosine residues, PCR site-directed mutagenesis was done by amplification of pACT ARIF-1 M1-D417 (full length) using primers to incorporate the desired mutation. Overlapping primers were used to generate proline-to-alanine mutations at ARIF-1 aa P303, P305, P309, P312, P328, P330, P335, P343, P351, P352, and P354, as well as tyrosine-to-phenylalanine mutations in ARIF-1 at aa Y226, Y238, Y241, Y246, Y320, Y325, and Y332. In all cases, the PCR product was purified by agarose gel electrophoresis, digested with *Dpn*I (New England Biolabs) to remove template DNA, transformed into XL-1 Blue *E. coli* (University of California,, Berkeley QB3 Macro Lab), and plated on LB agar plates with 100 μg/ml ampicillin (Life Technologies from Thermo Fisher Scientific). Plasmid DNA from resulting colonies was sequence-verified to ensure that the desired changes had been made.

To express BmNPV ARIF-1 with point mutations of proline and tyrosine residues, PCR site-directed mutagenesis was carried out as described above by amplification of pACT BmNPV ARIF-1 M1-N440 (full length) using primers to incorporate the desired mutation. Overlapping primers were used to generate proline-to-alanine mutations at BmNPV ARIF-1 aa P338, as well as tyrosine-to-phenylalanine mutations in BmNPV ARIF-1 at aa Y335. Colonies with the desired mutations were isolated as described above.

In all cases, to generate DNA ready for transfection, plasmids were transformed into JM109 *E. coli* and cultures grown in 150 ml 2× YT media (MilliporeSigma) overnight at 37°C. A Genelute endotoxin-free Maxiprep kit (MilliporeSigma; NA0410) was used to purify the DNA.

Plasmid construction for expression of GFP-tagged cortactin and Arp2/3 complex

To amplify the *S. frugiperda* cortactin gene, total mRNA was isolated from Sf21 cells using an RNeasy kit (Qiagen; 74004) and reverse-transcribed to cDNA using a Protoscript II First Strand DNA Synthesis kit (New England Biolabs; E6560S) using random hexamers as primers. *S. frugiperda* cortactin-specific primers were used to PCR-amplify a 1.9 kb fragment from cDNA that was then used as a template for PCR amplification with a second primer set. Next, we constructed a plasmid vector for an N-terminal GFP-tagged *S. frugiperda* cortactin. *eGFP* was PCR-amplified from pEGFP-N1 (Takara Bio USA) and inserted using Gibson assembly into a *Not*I/*Bam*HI-digested pACT. The amplified cortactin fragment was then subcloned into the *Not*I site of the resulting plasmid using Gibson assembly. The resulting plasmid expresses GFP fused to the N-terminus of *S. frugiperda* cortactin (GFP-cortactin). To express a fusion of EGFP to the C-terminus of the p21 (ARPC3) subunit of the Arp2/3 complex (p21-EGFP), the *T. ni arpc3* gene from pIZ-p21-EYFP (Goley *et al.*, 2006) was PCR-amplified and subcloned using Gibson assembly, along with *eGFP* PCR-amplified from pEGFP-N1 (Takara Bio USA), into the *Bam*HI site of pACT. In all cases, DNA ready for transfection was purified as described above.

ARIF-1 purification, anti–ARIF-1 antibody generation, and Western blotting

To express recombinant ARIF-1 protein in *E. coli*, the portion of the *arif-1* gene encoding the cytoplasmic C-terminal region (base pairs 654–1254, encoding the C-terminal 199 aa) was amplified by PCR from pEcoRI_ASalxh.pBSKS.rev and subcloned into the *Ssp*I site of pET-1M (University of California, Berkeley, QB3 Macro Lab) using Gibson cloning. This generated the plasmid pET-M1 ARIF-1 219 encoding a fusion protein of the predicted *arif-1* C-terminal cytoplasmic region with an N-terminal 6xHis tag, maltose-binding protein (MBP), and tobacco-etch virus (TEV) protease cleavage site (6xHi-MBP-TEV-ARIF-1-219-417). This plasmid was transformed into *E. coli* strain BL21(DE3) (New England Biolabs; C2527H), the bacteria were grown at 37°C to an OD_{600} of 0.5, and expression was induced with 250 μM IPTG for 2 h. Bacteria were harvested by centrifugation at 4000 rpm for 25 min at 4°C in a Beckman J6M clinical centrifuge (Beckman Coulter Diagnostics) and resuspended on ice in lysis buffer (50 mM Tris, pH 7.5, 200 mM KCl, 1 mM EDTA, 1 μg/ml each leupeptin, pepstatin, and chymostatin [LPC; MilliporeSigma], 1 μg/ml aprotinin [MP Biomedicals LLC], and 1 mM phenylmethylsulfonyl fluoride [PMSF; MilliporeSigma]). Lysozyme (MilliporeSigma) was added to the cells at 1 mg/ml; the bacteria were sonicated on ice at 30% power for 4 × 15 s in a Branson 450 Digital sonifier and centrifuged at 20,000 × *g* for 25 min using an SS34 rotor in a Sorvall RC 6+ centrifuge. The supernatant was dripped twice through a 10 ml packed volume of amylose resin (New England Biolabs; E8021S), washed with five column volumes of column buffer (20 mM Tris, pH 7.0, 200 mM NaCl), and eluted with column buffer containing 10 mM maltose. Fractions containing protein were pooled, and the protein concentration was determined by Bradford protein assay (Bio-Rad Laboratories).

Purified 6xHi-MBP-TEV-ARIF-1-219-417 was used to immunize rabbits (Pocono Rabbit Farm and Laboratory) using a 91-d protocol. Before affinity-purifying anti–ARIF-1 antibody, serum was first depleted of anti-MBP antibodies. Buffer exchange was carried out on 10 mg 6xHi-MBP-TEV, purified as described above using an Amicon Ultracell 10 kDa spin concentrator (MilliporeSigma) to concentrate the protein to 20 mg/ml in coupling buffer (0.2 M $NaHCO_3$, 500 mM NaCl, pH 8.0). This protein was coupled to a 1 ml packed column volume of NHS-activated Sepharose 4 Fast Flow resin (Cytiva Life Sciences; 17090601). Ten milliliters of serum was diluted 1:1 in binding buffer (20 mM Tris, pH 8.0), passed through a 0.22 μm filter, and passed over the MBP affinity resin six times at room temperature, and the flow-through was collected. Buffer exchange was carried out as described above to concentrate 10 mg of purified 6xHi-MBP-TEV-ARIF-1-219-417 to 10 mg/ml in coupling buffer. This protein was coupled to another 1 ml packed column volume of NHS-activated Sepharose 4 Fast Flow resin, and 10 ml of MBP antibody-depleted serum was passed over the 6xHi-MBP-TEV-ARIF-1-219-417 affinity

resin. Antibodies were eluted with 100 mM glycine, pH 2.5, and immediately brought to pH 7.5 by the addition of 1 M Tris, pH 8.8. Purified antibody was stored at –20°C.

To observe ARIF-1 expression over the course of early viral infection, Sf21 cells were infected with AcMNPV WOBpos, *Ac*Δ*arif-1*, and *Ac*Δ*arif-1-rescue* viruses at a multiplicity of infection (MOI) of 10 and harvested at 0, 2, 4, 6, 8, 10, 12, 16, 20, 24, 28, and 36 hpi. Cells were lysed in protein sample buffer (50 mM Tris, pH 6.8, 10 mM SDS, 370 µM bromophenol blue, 5% glycerol, 1 µg/ml LPC [MilliporeSigma], 1 µg/ml aprotinin [MP Biomedicals LLC], 1 mM PMSF [MilliporeSigma]) and boiled for 5 min. Cell lysates were subjected to SDS–PAGE, transferred to PVDF membrane (Immobilon from MilliporeSigma), and probed by Western blotting with rabbit anti–ARIF-1 and rabbit anti-cofilin loading control (provided by Kris Gunsalus, New York University–Abu Dhabi, and Michael Goldberg, Cornell).

To observe expression of ARIF-1 and its truncated and mutated derivatives, adherent Sf21 cells were transfected with plasmids expressing ARIF-1 using TransIT-Insect transfection reagent (Mirus Bio). At 3 d posttransfection, cells were collected, lysed in protein sample buffer (0.2 M Tris HCl, 0.4 M dithiothreitol [DTT], 277 mM SDS, 6 mM bromophenol blue, 4.3 M glycerol), and boiled and subjected to SDS–PAGE and Western blotting as described above.

Fluorescence microscopy

To image actin structures in live infected cells, Sf21 cells were plated onto 35 mm dishes with 20 mm diameter no 1.5 glass coverslips (MatTek; P35G-1.5-20-C) and incubated overnight at 28°C in Grace's media with 10% FBS (Gemini Bio-Products). Cells were transfected with 5 µg of pACT-GFP-actin using TransIT-Insect transfection reagent (Mirus Bio) and incubated for 2 d at 28°C in Grace's media with 10% FBS and antibiotics (100 µg/ml penicillin/streptomycin and 0.25 µg/ml amphotericin B). Cells were infected with virus at an MOI of 10, and after 1 h adsorption at 28°C, they were washed with Grace's media with 10% FBS (this point is defined as 0 hpi) and incubated at 28°C in Grace's media with 10% FBS and antibiotics/antimycotics until imaging.

To image actin structures in live cells, Sf21 cells were plated as described above and cotransfected with 5 µg of pACT-ARIF-1 or its truncated or mutated derivatives, pACT-GFP-ARIF-1, pACT-GFP-P21, or pACT-GFP-Cortactin. Cells were incubated for 2 d at 28°C in Grace's media with 10% FBS and antibiotics/antimycotics and imaged.

To image endogenous ARIF-1, Sf21 cells were plated in a six-well dish on 22 × 22 1.5 coverslips and incubated overnight at 28°C in Grace's media with 10% FBS (Gemini Bio-Products). Cells were infected with virus at an MOI of 10, and after 1 h adsorption at 28°C, they were washed with Grace's media with 10% FBS and incubated at 28°C in Grace's media with 10% FBS and antibiotics/antimycotics for 5 h. Cells were fixed in 4% paraformaldehyde in PHEM buffer (60 mM PIPES, pH 6.9, 25 mM HEPES, 10 mM EGTA [ethylene glycol-bis(2-aminoethylether)-*N*,*N*,*N*′,*N*′-tetraacetic acid], 2 mM $MgCl_2$), quenched with 0.1 M glycine in PHEM buffer, permeabilized in 0.15% Triton X-100 in PHEM buffer, and blocked with 5% normal goat serum (MP Biomedicals; 08642921) in PHEM. Cells were stained with anti–ARIF-1 primary antibody (generated as described above) at a 1:100 dilution in PHEM buffer and with a goat anti rabbit Alexa Fluor 488–conjugated secondary antibody (Invitrogen from Thermo Fisher Scientific; A27034) diluted 1:500 in PHEM buffer. F-actin was visualized with Alexa Fluor 568 phalloidin (Invitrogen from Thermo Fisher Scientific; A12380) diluted 1:400 in PHEM buffer.

To quantify the formation of invadosome clusters in Sf21 cells transfected with pACT-ARIF-1, without or with truncations and mutations, cells were transfected as described above. At 2 d posttransfection, 60 random cells per condition expressing visible GFP-actin were imaged in triplicate at one *Z* plane at the basal side of the cell. The number of cells with invadosome clusters, the number of invadosome clusters in each cell, and the shape of the invadosome clusters were recorded. The data are a result of three biological replicates.

Imaging was performed using a Nikon/Andor confocal microscope with a Yokogawa CSU-XI spinning disk, a Clara Interline CCD camera (Oxford Instruments), and MetaMorph software 7.8.2.0 (Molecular Devices LLC) using a 100× VC objective and a 488 nm excitation laser, as well as a Zeiss Laser Scanning Microscope 880 with Airyscan Fast module (Carl Zeiss AG) and Zen Black ver. 3.3 and Zen Blue ver. 3.3 software (Zeiss AG) using a 40× water objective and 488 and 561 nm excitation lasers. TIRF imaging was performed on a Leica DMi8 S Infinity TIRF HP system with a 100×/1.47 TIRF oil immersion objective and a 488 nm excitation laser and detected with a Hamamatsu Flash V.4.0 sCMOS camera. Images were processed using ImageJ ver. 1.53 software.

To quantify invadosome cluster formation in infected cells over a time course, Sf21 cells were plated onto µclear CELLSTAR black-walled 96-well plates (Greiner Bio-One; 655086) and infected at an MOI of 10 with WOBpos, *Ac*Δ*arif-1*, or *Ac*Δ*arif-1-rescue* virus as described above. Cells were fixed with 4% paraformaldehyde in PHEM buffer, quenched with 0.1 M glycine in PHEM buffer, permeabilized in 0.15% Triton X-100 in PHEM buffer, and blocked with 5% normal goat serum (MP Biomedicals) and 1% bovine serum albumin in PHEM. Cells were stained with anti-GP64 B12D5 primary antibody (a gift from Loy Volkman) at a 1:200 dilution in PHEM buffer and with a secondary goat anti-mouse Alexa Fluor 488–conjugated antibody (Invitrogen from Thermo Fisher Scientific) at a 1:400 dilution, also in PHEM buffer. F-actin was visualized with Alexa Fluor 568 phalloidin (Invitrogen from Thermo Fisher Scientific) diluted 1:200 in PHEM buffer, and DNA was visualized with 5 µg/ml Hoechst (MilliporeSigma) in PHEM buffer. Cells were imaged with an Opera Phenix high-content image screening system (PerkinElmer) using a 40× water immersion objective (PerkinElmer). Images were analyzed on Harmony ver. 4.8 image analysis software (PerkinElmer) using maximum intensity projections, and the number of cells, number of cells with GP64 signal, number of cells with invadosome clusters, and number of clusters of invadosome clusters in each cell were recorded. The data are a result of three biological replicates.

For Arp2/3 complex drug inhibition experiments, Sf21 cells were plated and transfected with pACT-GFP-actin as described above. Cells were infected with AcMNPV WOBpos at an MOI of 10 as described above, and at 4 hpi, latrunculin A in dimethyl sulfoxide (DMSO) was added to a final concentration of 4 µM, or CK666 (MilliporeSigma; 182515) or CK689 (MilliporeSigma; 182517) in DMSO was added to a final concentration of 100 µM. Imaging was begun immediately, with eight cells imaged every 30 s. Images were processed with ImageJ ver. 1.53 software, and the percent of invadosome clusters remaining was recorded. The data are a result of three biological replicates.

Matrix degradation experiments

Matrix degradation experiments were carried out using a modified protocol from Artym *et al.* (2009). Briefly, 50 µg poly-L-lysine (MilliporeSigma; A-005-C) was added to 35 mm dishes containing 20 mm diameter no 1.5 glass coverslips (MatTek) and incubated for 1 h at room temperature. A 2.5% wt/wt solution of both sucrose and bovine skin gelatin (MilliporeSigma; G6650) at 37°C was added, excess solution was removed, and dishes were incubated for 10 min at

room temperature. Next, the dishes were washed three times with Dulbecco's phosphate-buffered saline without calcium and magnesium (DPBS; Life Technologies; 14190250) and incubated for 15 min in ice-cold 0.5% glutaraldehyde (MilliporeSigma; 354400) in DPBS. The dishes were washed again three times with DPBS, and 50 µg/ml rhodamine-fibronectin (Cytoskeleton; FNR01) was added and incubated in the dark at room temperature for 2 h. Next, Grace's media with 10% FBS and antibiotics/antimycotics was added to the dishes and incubated at 28°C for 1 h. Sf21 cells were plated onto dishes and incubated for 4 d. Cells were transfected with GFP-actin as described above, and 2 d posttransfection they were infected with Ac-MNPV WOBpos at an MOI of 10 or mock infected. Coverslip dishes were imaged on a Zeiss Laser Scanning Microscope 880 with Airyscan Fast module with a 40× water objective (Carl Zeiss AG) with 488 and 510 nm excitation lasers starting at 3 hpi every 15 min for 5 h. Files were deconvolved using Zen Black ver. 3.3 software (Carl Zeiss AG). ImageJ ver. 1.53 software was used to measure the integrated signal intensity of GFP-actin in individual invadosome clusters and the corresponding areas of the underlying rhodamine fibronectin over the time course. Data were normalized to area, and the background was subtracted. The correlation between actin and rhodamine-fibronectin signal over time was determined through Pearson correlation tests using GraphPad Prism ver. 7.04, and the correlation coefficients were computed and plotted for each treatment.

ACKNOWLEDGMENTS

We thank the following individuals for their contributions to this work: Loy Volkman for her advice, support, and role as a pioneer in the field of baculovirus host–pathogen interactions; Mary West and Chris Noel of the UC Berkeley QB3 High-Throughput Screening facility for the use of facilities and technical support; Holly Aaron and Jen-Yi Lee of the UC Berkeley Molecular Imaging Center for support for our microscopy work; David Acevedo, Alienor Baskevitch, Varsha Rajshekar, and Gary Karpen for additional microscopy support; Michael Goldberg and Kris Gunsalus for the rabbit anti–cofilin GA15 antibody; Susan Hepp and Bisco Hill for providing plasmid constructs and advice. This work was supported by Grant R35 GM127108 from the National Institutes of Health (NIH)/National Institute of General Medical Sciences to M.D.W. and Grant 1S10OD021828-01A1 from the NIH Office of the Director, which funded the Opera Phenix microscope.

REFERENCES

Abram CL, Seals DF, Pass I, Salinsky D, Maurer L, Roth TM, Courtneidge SA (2003). The adaptor protein Fish associates with the members of the ADAMs family and localizes to podosomes of SRC-transformed cells. J Biol Chem 278, 16844–16851.

Artym VV, Yamada KM, Mueller SC (2009). ECM degradation assays for analyzing local cell invasion. Methods Mol Bio 522, 211–219.

Buday L, Wunderlich L, Tamás P (2002). The Nck family of adapter proteins: regulators of actin cytoskeleton. Cell Signal 14, 723–731.

Burger KL, Learman BS, Boucherle AK, Sirintrapun SJ, Isom S, Díaz B, Courtneidge SA, Seals DF (2014). Src-dependent Tks5 phosphorylation regulates invadopodia-associated invasion in prostate cancer cells: Tks5 phosphorylation and cell invasion. Prostate 74, 134–148.

Burgstaller G, Gimona M (2005). Podosome-mediated matrix resorption and cell motility in vascular smooth muscle cells. Am J Physiol Heart Circ Physiol 288, H3001–H3005.

Burns S, Thrasher AJ, Blundell MP, Machesky L, Jones GE (2001). Configuration of human dendritic cell cytoskeleton by Rho GTPases, the WAS protein, and differentiation. Blood 98, 1142–1149.

Castro-Castro A, Marchesin V, Monteiro P, Lodillinsky C, Rossé C, Chavrier P (2016). Cellular and molecular mechanisms of MT1-MMP-dependent cancer cell invasion. Annu Rev Cell Dev Biol 32, 555–576.

Charlton CA, Volkman LE (1991). Sequential rearrangement and nuclear polymerization of actin in baculovirus-infected *Spodoptera frugiperda* cells. J Virol 65, 1219–1227.

Charlton CA, Volkman LE (1993). Penetration of *Autographa californica* nuclear polyhedrosis virus nucleocapsids into IPLB Sf 21 cells induces actin cable formation. Virology 197, 245–254.

Chen WT (1989). Proteolytic activity of specialized surface protrusions formed at rosette contact sites of transformed cells. J Exp Zool 251, 167–185.

Chen WT, Chen JM, Parsons SJ, Parsons JT (1985). Local degradation of fibronectin at sites of expression of the transforming gene product pp60src. Nature 316, 156–158.

Datsenko KA, Wanner BL (2000). One-step inactivation of chromosomal genes in *Escherichia coli* K-12 using PCR products. Proc Natl Acad Sci USA 97, 6640–6645.

David-Pfeuty T, Singer SJ (1980). Altered distributions of the cytoskeletal proteins vinculin and α-actinin in cultured fibroblasts transformed by Rous sarcoma virus. Proc Natl Acad Sci USA 77, 6687–6691.

Destaing O, Saltel F, Geminard JC, Jurdic P, Bard F (2003). Podosomes display actin turnover and dynamic self-organization in osteoclasts expressing actin-green fluorescent protein. Mol Biol Cell 14, 407–416.

Detvisitsakun C, Berretta MF, Lehiy C, Passarelli AL (2005). Stimulation of cell motility by viral fibroblast growth factor homolog: proposal for a role in viral pathogenesis. Virology 366, 308–317.

Detvisitsakun C, Cain EL, Passarelli AL (2007). The *Autographa californica* M nucleopolyhedrovirus fibroblast growth factor accelerates host mortality. Virology 365, 70–78.

Di Martino J, Paysan L, Gest C, Lagrée V, Juin A, Saltel F, Moreau V (2014). Cdc42 and Tks5: a minimal and universal molecular signature for functional invadosomes. Cell Adhes Migr 8, 280–292.

Dreschers S, Roncarati R, Knebel-Mörsdorf D (2001). Actin rearrangement-inducing factor of baculoviruses is tyrosine phosphorylated and colocalizes to F-actin at the plasma membrane. J Virol 75, 3771–3778.

Eddy RJ, Weidmann MD, Sharma VP, Condeelis JS (2017). Tumor cell invadopodia: invasive protrusions that orchestrate metastasis. Trends Cell Biol 27, 595–607.

Engelhard EK, Kam-Morgan LN, Washburn JO, Volkman LE (1994). The insect tracheal system: a conduit for the systemic spread of *Autographa californica* M nuclear polyhedrosis virus. Proc Natl Acad Sci USA 91, 3224–3227.

Filippakopoulos P, Müller S, Knapp S (2009). SH2 domains: modulators of nonreceptor tyrosine kinase activity. Curr Opin Struc Biol 19, 643–649.

Gibson D, Young L, Chuang RY, Venter JC, Hutchison CA 3rd, Smith HO (2009). Enzymatic assembly of DNA molecules up to several hundred kilobases. Nat Methods 6, 343–345.

Goley ED, Ohkawa T, Mancuso J, Woodruff JB, D'Alessio JA, Cande WZ, Volkman LE, Welch MD (2006). Dynamic nuclear actin assembly by Arp2/3 complex and a baculovirus WASP-like protein. Science 314, 464–467.

Granados RR, Lawler KA (1981). In vivo pathway of *Autographa californica* baculovirus invasion and infection. Virology 108, 297–308.

Hai CM, Hahne P, Harrington EO, Gimona M (2002). Conventional protein kinase C mediates phorbol-dibutyrate-induced cytoskeletal remodeling in A7r5 smooth muscle cells. Exp Cell Res 280, 64–74.

Haralalka S, Shelton C, Cartwright HN, Katzfey E, Janzen E, Abmayr SM (2011). Asymmetric Mbc, active rac1 and F-actin foci in the fusion-competent myoblasts during myoblast fusion in *Drosophila*. Development 138, 1551–1562.

Hepp SE, Borgo GM, Ticau S, Ohkawa T, Welch MD (2018). Baculovirus AC102 is a nucleocapsid protein that is crucial for nuclear actin polymerization and nucleocapsid morphogenesis. J Virol 92, e00111.

Hess RT, Falcon LA (1987). Temporal events in the invasion of the codling moth, *Cydia pomonella*, by a granulosis virus: an electron microscope study. J Invertebr Pathol 50, 85–105.

Hess RT, Goldsmith PA, Volkman LE (1989). Effect of cytochalasin D on cell morphology and AcMNPV replication in a *Spodoptera frugiperda* cell line. J Invertebr Pathol 53, 169–182.

Hiura K, Lim SS, Little SP, Lin S, Sato M (1995). Differentiation dependent expression of tensin and cortactin in chicken osteoclasts. Cell Motil Cytoskel 30, 272–284.

Ishimwe E, Hodgeson JJ, Clem RJ, Passarelli AL (2016). Reaching the melting point: degradative enzymes and protease inhibitors involved in baculovirus infection and dissemination. J Virol 479, 637–649.

Kanner SB, Reynolds AB, Vines RR, Parsons JT (1990). Monoclonal antibodies to individual tyrosine-phosphorylated protein substrates of oncogene-encoded tyrosine kinases. Proc Natl Acad Sci USA 87, 3328–3332.

Katsuma S, Daimon T, Mita K, Shimada T (2006). Lepidopteran ortholog of *Drosophila* breathless is a receptor for the baculovirus fibroblast growth factor. J Virol 80, 5474–5481.
Katsuma S, Shimada T, Kobayashi M (2004). Characterization of the baculovirus *Bombyx mori* nucleopolyhedrovirus gene homologous to the mammalian FGF gene family. Virus Genes 29, 211–217.
Kelly T, Mueller SC, Yeh Y, Chen W (1994). Invadopodia promote proteolysis of a wide variety of extracellular matrix proteins. J Cell Physiol 158, 299–308.
Kokusho R, Kawamoto M, Koyano Y, Sugano S, Suzuki Y, Shimada T, Katsuma S (2015). *Bombyx mori* nucleopolyhedrovirus actin rearrangement-inducing factor 1 enhances systemic infection in *B. mori* larvae. J Gen Virol 96, 1938–1946.
Kuo SL, Chen CL, Pan YR, Chiu WT, Chen HC (2018). Biogenesis of podosome rosettes through fission. Sci Rep 8, 524.
Lehiy C, Martinez O, Passarelli AL (2009). Virion-associated viral fibroblast growth factor stimulates cell motility. Virology 395, 152–160.
Linder S, Higgs H, Hüfner K, Schwarz K, Pannicke U, Aepfelbacher M (2000). The polarization defect of Wiskott-Aldrich syndrome macrophages is linked to dislocalization of the Arp2/3 complex. J Immunol 165, 221–225.
Linder S, Nelson D, Weiss M, Aepfelbacher M (1999). Wiskott-Aldrich syndrome protein regulates podosomes in primary human macrophages. Proc Natl Acad Sci USA 96, 9648–9653.
Linder S, Wiesner C, Himmal M (2011). Degrading devices: invadosomes in proteolytic cell invasion. Annu Rev Cell Dev Biol. 27, 185–211.
Luxenburg C, Geblinger D, Klein E, Anderson K, Hanein D, Geiger B, Addadi L (2007). The architecture of the adhesive apparatus of cultured osteoclasts: from podosome formation to sealing zone assembly. PLoS One 2, e179.
Marchisio P (1987). Rous sarcoma virus-transformed fibroblasts and cells of monocytic origin display a peculiar dot-like organization of cytoskeletal proteins involved in microfilament-membrane interactions. Exp Cell Res 169, 202–214.
Marchisio PC, Cirillo D, Naldini L, Primavera MV, Teti A, Zambonin-Zallone A (1984). Cell-substratum interaction of cultured avian osteoclasts is mediated by specific adhesion structures. J Cell Biol 99, 1696–1705.
Means JC, Passarelli AL (2010). Viral fibroblast growth factor, matrix metalloproteases, and caspases are associated with enhancing systemic infection by baculoviruses. Proc Natl Acad Sci USA 107, 9825–9830.
Mizutani K, Miki H, He H, Maruta H, Takenawa T (2002). Essential role of neural Wiskott-Aldrich syndrome protein in podosome formation and degradation of extracellular matrix in src-transformed fibroblasts. Cancer Res 62, 669–674.
Monsky WL, Lin CY, Aoyama A, Kelly T, Akiyama SK, Mueller SC, Chen WT (1994). A potential marker protease of invasiveness, seprase, is localized on invadopodia of human malignant melanoma cells. Cancer Res 54, 5702–5710.
Moreau V, Tatin F, Varon C, Génot E (2003). Actin can reorganize into podosomes in aortic endothelial cells, a process controlled by Cdc42 and RhoA. Mol Cell Biol 23, 6809–6822.
Mueller SC, Ghersi G, Akiyama SK, Sang QXA, Howard L, Pineiro-Sanchez M, Nakahara H, Yeh Y, Chen WT (1999). A novel protease-docking function of integrin at invadopodia. J Biol Chem 274, 24947–24952.
Murphy DA, Courtneidge SA (2011). The 'ins' and 'outs' of podosomes and invadopodia: characteristics, formation and function. Nat Rev Mol Cell Biol 12, 413–426.
Nermut MV, Eason P, Hirst EMA, Kellie S (1991). Cell/substratum adhesions in RSV-transformed rat fibroblasts. Exp Cell Res 193, 382–397.
Ohkawa T, Rowe AR, Volkman LE (2002). Identification of six *Autographa californica* multicapsid nucleopolyhedrovirus early genes that mediate nuclear localization of G-actin. J Virol 76, 12281–12289.
Ohkawa T, Volkman LE (1999). Nuclear F-actin is required for AcMNPV nucleocapsid morphogenesis. Virology 264, 1–4.
Ohkawa T, Volkman LE, Welch MD (2010). Actin-based motility drives baculovirus transit to the nucleus and cell surface. J Cell Biol 190, 187–195.
Ohkawa T, Washburn JO, Sitapara R, Sid E, Volkman LE (2005). Specific binding of *Autographa californica* M nucleopolyhedrovirus occlusion-derived virus to midgut cells of *Heliothis virescens* larvae is mediated by products of *pif* genes *Ac119* and *Ac022* but not by *Ac115*. J Virol 79, 15258–15264.
Ohkawa T, Welch MD (2018). Baculovirus actin-based motility drives nuclear envelope disruption and nuclear egress. Curr Biol 28, 2153–2159.e4.
Onel SF, Renkawitz-Pohl R (2009). FuRMAS: triggering myoblast fusion in *Drosophila*. Dev Dynam 238, 1513–1525.
Oser M, Yamaguchi H, Mader CC, Bravo-Cordero JJ, Arias M, Chen X, DesMarais V, van Rheenen J, Koleske AJ, Condeelis J (2009). Cortactin regulates cofilin and N-WASp activities to control the stages of invadopodium assembly and maturation. J Cell Biol 186, 571–587.
Passarelli AL (2011). Barriers to success: how baculoviruses establish efficient systemic infections. Virology 411, 383–392.
Paz H, Pathak N, Yang J (2014). Invading one step at a time: the role of invadopodia in tumor metastasis. Oncogene 33, 4193–4202.
Reddy JT, Locke M (1990). The size limited penetration of gold particles through insect basal laminae. J Insect Physiol 36, 397–407.
Rohrmann GF (2019). Baculovirus Molecular Biology, 4th Ed,. Bethesda, MD: National Center for Biotechnology Information. Available from https://www.ncbi.nlm.nih.gov/books/NBK543458.
Roncarati R, Knebel-Mörsdorf D (1997). Identification of the early actin-rearrangement-inducing factor gene, *arif-1*, from *Autographa californica* multicapsid nuclear polyhedrosis virus. J Virol 72, 888–889.
Schuuring E, Verhoeven E, Litvinov S, Michalides RJ (1993). The product of the EMS1 gene, amplified and overexpressed in human carcinomas, is homologous to a v-src substrate and is located in cell-substratum contact sites. Mol Cell Biol 13, 2891–2898.
Seals DF, Azucena EF, Pass I, Tesfay L, Gordon R, Woodrow M, Resau JH, Courtneidge SA (2005). The adaptor protein Tks5/Fish is required for podosome formation and function, and for the protease-driven invasion of cancer cells. Cancer Cell 7, 155–165.
Sens KL, Zhang S, Jin P, Duan R, Zhang G, Luo F, Parachini L, Chen EH (2010). An invasive podosome-like structure promotes fusion pore formation during myoblast fusion. J Cell Biol 191, 1013–1027.
Stickel SK, Wang YL (1987). Alpha-actinin-containing aggregates in transformed cells are highly dynamic structures. J Cell Biol 104, 1521–1526.
Stylli SS, Stacey TTI, Verhagen AM, Xu SS, Pass I, Courtneidge SA, Lock P (2009). Nck adaptor proteins link Tks5 to invadopodia actin regulation and ECM degradation. J Cell Sci 122, 2727–2740.
Taka H, Ono C, Sato M, Asano S, Bando H (2013). Complex genetic interactions among non-essential genes of BmNPV revealed by multiple gene knockout analysis. J Insect Biotechnol Sericol 82, 25–32.
Tarone G, Cirillo D, Giancotti FG, Comoglio PM, Marchisio PC (1985). Rous sarcoma virus-transformed fibroblasts adhere primarily at discrete protrusions of the ventral membrane called podosomes. Exp Cell Res 159, 141–157.
Tu C, Ortega-Cava CF, Chen G, Fernandes ND, Cavallo-Medved D, Sloane BF, Band V, Band H (2008). Lysosomal cathepsin B participates in the podosome-mediated extracellular matrix degradation and invasion via secreted lysosomes in v-Src fibroblasts. Cancer Res 68, 9147–9156.
Varon C, Tatin F, Moreau V, Van Obberghen-Schilling E, Fernandez-Sauze S, Reuzeau E, Kramer I, Génot E (2006). Transforming growth factor β induces rosettes of podosomes in primary aortic endothelial cells. Mol Cell Biol 26, 3582–3594.
Volkman L, Talhouk S, Oppenheimer D, Charlton CA (1992). Nuclear F-actin: a functional component of baculovirus-infected lepidopteran cells? J Cell Sci 103, 15–22.
Volkman LE (1988). *Autographa californica* MNPV nucleocapsid assembly: inhibition by cytochalasin D. Virology 163, 547–553.
Volkman LE, Goldsmith PA, Hess RT (1987). Evidence for microfilament involvement in budded *Autographa californica* nuclear polyhedrosis virus production. Virology 156, 32–39.
Volkman LE, Kasman LM (2000). Filamentous actin is required for lepidopteran nucleopolyhedrovirus progeny production. J Gen Virol 81, 1881–1888.
Weaver SC, Scott TW, Lorenz LH, Lerdthusnee K, Romoser WS (1988). Togavirus-associated pathologic changes in the midgut of a natural mosquito vector. J Virol 62, 2083–2090.
Webb BA, Eves R, Crawley SW, Zhou S, Côté GP, Mak AS (2005). PAK1 induces podosome formation in A7r5 vascular smooth muscle cells in a PAK-interacting exchange factor-dependent manner. Am J Physiol Cell Physiol 289, C898–C907.
Yamaguchi H, Lorenz M, Kempiak S, Sarmiento C, Coniglio S, Symons M, Segall J, Eddy R, Miki H, Takenawa T, Condeelis J (2005). Molecular mechanisms of invadopodium formation. J Cell Biol 168, 441–452.
Zhou S, Webb BA, Eves R, Mak AS (2006). Effects of tyrosine phosphorylation of cortactin on podosome formation in A7r5 vascular smooth muscle cells. Am J Physiol Cell Physiol 290, C463–C471.